Environmental Fluid Mechanics
https://doi.org/10.1007/s10652-019-09682-0

ORIGINAL ARTICLE

Hydraulics of shallow shear flows: onset, development and practical relevance

M. Y. Lam[1] · **M. S. Ghidaoui**[2] · **A. A. Kolyshkin**[3]

Received: 29 May 2018 / Accepted: 21 March 2019

Abstract
Shallow turbulent flows are omnipresent in hydrosystems. Examples include flows past islands, in river confluences and longshore currents. A characteristic feature of a shallow flow is the existence (under certain conditions) of two-dimensional coherent structures (2DCS). This paper discusses and illustrates the usefulness and limitations of reduced dimensionality models in conjunction with hydrodynamic stability theories in illuminating the onset and subsequent dynamics of 2DCS in shallow flows. The paper follows closely the keynote lecture given by the second author on the 4th International Symposium on Shallow Flows which took place in Eindhoven in 2017. The paper gives the reader a comprehensive review of the reduced dimensionality models and hydrodynamic stability theories used in analyzing the dynamics of shallow flows.

Keywords Shallow flows · Coherent structures · Stability theories

1 Introduction

Shallow turbulent flows are flows with horizontal turbulent lengthscale far greater than the water depth. Turbulence development is vertically constrained by the water depth but is horizontally unconstrained. Such a confinement separates the turbulent flow into large-scale two-dimensional turbulence and small-scale three-dimensional turbulence. In an environmental hydraulics setting, the thin water layer is usually bounded by a frictional bottom and a free surface. Horizontal velocity gradients, which generate horizontal turbulence, are also usually present in the flows. Jirka and Uijttewaal [35] define shallow flows as "largely unidirectional, turbulent shear flows occuring in a confined layer of depth scale H. This confinement leads to a separation of turbulent motions between small scale three-dimensional

✉ M. Y. Lam
celmy@connect.ust.hk

A. A. Kolyshkin
andrejs.koliskins@rtu.lv

[1] Hong Kong University of Science and Technology, Room 1210, Clear Water Bay, Hong Kong

[2] Hong Kong University of Science and Technology, Room 3569, Clear Water Bay, Hong Kong

[3] Riga Technical University, Room D2-135, Riga, Latvia

Published online: 01 April 2019

turbulence, $L_{3D} < H$, and large scale two-dimensional turbulent motions, $L_{2D} > H$ with mutual interaction." A characteristic feature of shallow flows is the presence of horizontal two-dimensional coherent structures (2DCS). 2DCS are defined [36] as "connected large-scale turbulent fluid masses that extend uniformly over the full water depth and contain a phase correlated vorticity (with the exception of a thin near-bottom boundary layer)". Jirka [36] proposed three 2DCS generating mechanisms:

- *Type A (topographic forcing)* Topographic features (e.g. headlands and islands) leading to local flow separation, giving rise to strong horizontal shear layers.
- *Type B (internal transverse shear instabilities)* Velocity variations in the flow (e.g. source flows having a momentum excess or deficit, horizontal changes in bottom roughness) resulting to a gradual growth of 2DCS.
- *Type C (secondary instabilities of the base flow)* Formation of 2DCS due to the imbalance of boundary layer type turbulence caused by e.g. localized roughness zones.

Among the mechanisms, type A is the strongest and type C is the weakest with limited experimental evidence. Chan [8] showed that the effect of topographic features is to generate a horizontal shear layer, which is the fundamental driving force of 2DCS. The dissipative force is the bed friction. The ratio of the dissipative force to the driving force plays an important role in the development of instability. 2DCS are formed if this ratio is much smaller than unity. As 2DCS travel downstream this ratio increases gradually, eventually leading to a stable flow.

Shallow turbulent flows are omnipresent in hydrosystems. Two examples of such flows are shallow wakes and shallow mixing layers. Shallow wakes are flows past obstacles, e.g. islands, under water depth confinement and bed friction. For example, the horizontal scale of the eddies in the wake of Rattray Island in northeast Australia is of the order of 1000 m, while the water depth is of the order of 20 m [75]. In addition, the horizontal scale of the eddies in the wake of islands in Rupert Bay in northern Canada ranges from 100 to 3000 m, while water depth ranges from 1 to 4 m [34]. Shallow mixing layers are flow configurations in which two streams with different velocities come into contact under water depth confinement. For example, the horizontal scale of the eddies in the mixing layer downstream of a junction of the Mekong river is of the order of 1000 m, while the water depth ranges from 5 to 10 m [37].

Shallow flows exhibit features of two-dimensionality. For example, experimental investigation of plane turbulent jets in a bounded fluid layer [19] suggests that the flow is largely two-dimensional beyond a streamwise distance of ten fluid layer depths. The subsequent development of 2DCS is described by the theory of two-dimensional turbulence (see [46, 50]). Thus, researchers usually employ reduced dimensionality models to study shallow flows. Simulations by reduced dimensionality models of shallow flows have been conducted in [25, 73]. Features of shallow shear flows, e.g. 2DCS size and frequency of flow oscillations, were successfully reproduced. Hydrodynamic stability theories based on two dimensional models have also been used to illuminate key physics of shallow flows with good success [11, 16, 25, 45, 72].

The paper is based on the keynote presentation of the second author on the 4th International Symposium on Shallow Flows which took place in Eindhoven in 2017. The objective of the paper is to give the reader a comprehensive review of the methods and theories used to analyse the dynamics of shallow flows. The paper is organized as follows. Governing equations are presented in Sect. 2 where the limitations and domains of validity of reduced dimensionality models are discussed. Section 3 is devoted to hydrodynamic stability theory in the

context of shallow flows. A review of linear and weakly nonlinear theories is given. In addition, the mean field theory and secondary instability theory are presented. Sections 4, 5 and 6 are devoted to the application of the methods and theories discussed above. Application to shallow wakes are discussed in Sect. 4. Concepts of absolute and convective instabilities in the context of the classification of flow patterns behind obstacles as well as frequency selection criteria are analyzed. Section 5 is devoted to the analysis of shallow mixing layers from a hydrodynamic stability point of view. Linear theory as well as secondary instability theory and mean field theory are applied to analyze the dynamics of shallow mixing layers. Finally, in Sect. 6 the effect of the Froude number on the stability and development of shallow mixing layers is analyzed. This paper provides an overview to the topic. Readers are referred to the references for details.

2 Governing equations and reduced dimensionality models

Some phenomena observed in shallow flows resemble flow structures that occur in two-dimensional hydrodynamics for small Reynolds numbers. Wolansky et al. [75] and Ingram and Chu [34] observed large scale two-dimensional vortex street and unsteady bubbles in the lee of islands under a Reynolds number of 10^7. Vortex merging, spatial growth of dominant length scale and a -3 spectral slope is observed in shallow jets, mixing layers and dipoles in shallow water (e.g., [1, 2, 19, 69, 70]). These observations suggest that large scale motion in shallow water can be described by reduced dimensionality models (2-D shallow flow models or integral models). Such models usually well describe the large scale physics, for example, spreading, velocity profiles, oscillation frequencies, eddy structures, etc (see [7, 11, 30, 41, 53, 57, 72]). Two dimensional linear stability analysis explain well the transition between different observed flow regimes [11, 12, 16, 23, 25, 45, 47, 72].

2.1 Reduced dimensionality model for a shallow and small Froude number flow

Consider the three-dimensional Navier Stokes equations and their boundary conditions in free surface flows:

$$\frac{\partial u}{\partial x}+\frac{\partial v}{\partial y}+\frac{\partial w}{\partial z}=0, \tag{1}$$

$$\frac{\partial u}{\partial t}+\frac{\partial uu}{\partial x}+\frac{\partial uv}{\partial y}+\frac{\partial uw}{\partial z}=-\frac{1}{\rho}\frac{\partial p}{\partial x}+\nu\left(\frac{\partial^2 u}{\partial x^2}+\frac{\partial^2 u}{\partial y^2}+\frac{\partial^2 u}{\partial z^2}\right), \tag{2}$$

$$\frac{\partial v}{\partial t}+\frac{\partial vu}{\partial x}+\frac{\partial vv}{\partial y}+\frac{\partial vw}{\partial z}=-\frac{1}{\rho}\frac{\partial p}{\partial y}+\nu\left(\frac{\partial^2 v}{\partial x^2}+\frac{\partial^2 v}{\partial y^2}+\frac{\partial^2 v}{\partial z^2}\right), \tag{3}$$

$$\frac{\partial w}{\partial t}+\frac{\partial wu}{\partial x}+\frac{\partial wv}{\partial y}+\frac{\partial ww}{\partial z}=-\frac{1}{\rho}\frac{\partial p}{\partial z}-g+\nu\left(\frac{\partial^2 w}{\partial x^2}+\frac{\partial^2 w}{\partial y^2}+\frac{\partial^2 w}{\partial z^2}\right), \tag{4}$$

$$\frac{\partial \eta}{\partial t}+u\frac{\partial \eta}{\partial x}+v\frac{\partial \eta}{\partial y}=w_{surface}, \tag{5}$$

$$u(x, y, 0, t) = v(x, y, 0, t) = w(x, y, 0, t) = 0 \tag{6}$$

where x, y and z are the two horizontal and the vertical coordinates respectively; $u(x, y, z, t)$, $v(x, y, z, t)$, $w(x, y, z, t)$ are the velocity along x, y and z; $p(x, y, z, t)$ is pressure; $\eta(x, y, t)$ is free-surface elevation; g is gravitational acceleration; ν is viscosity. Equation (1) is the mass conservation equation; Eqs. (2–4) are the momentum equations; Eq. (5) is the kinematic boundary condition at the free-surface; and Eq. (6) represent the zero flux and no-slip conditions at the bed.

Let L be the horizontal lengthscale, H the water depth, U the horizontal velocity scale, W the vertical velocity scale, and $T = L/U$ the time scale. Equation (1) dictates that W is of order UH/L. Combining this result, the fact the wave amplitude scale is $\frac{U\sqrt{gH}}{g}$ [17] and Eq. (5) gives

$$Fr\left(\frac{\partial \eta^*}{\partial T^*} + U^*\frac{\partial \eta^*}{\partial X^*} + V^*\frac{\partial \eta^*}{\partial Y^*}\right) = W^* \tag{7}$$

superscript $*$ denotes dimensionless quantities and $Fr = U/\sqrt{gH}$. Therefore, $W \to 0$ as $Fr \to 0$ implying that the free-surface becomes a rigid lid when $Fr \to 0$. Imposing $W = 0$ at the free surface, integrating the Navier–Stokes equations with respect to depth, neglecting the shear stresses at the free surface and assuming the bed shear stresses are modeled by the quadratic friction formula gives the following rigid-lid shallow water equations

$$\frac{\partial \bar{u}}{\partial x} + \frac{\partial \bar{v}}{\partial y} = 0, \tag{8}$$

$$\frac{\partial \bar{u}}{\partial t} + \bar{u}\frac{\partial \bar{u}}{\partial x} + \bar{v}\frac{\partial \bar{u}}{\partial y} = -\frac{\partial \bar{p}}{\partial x} - \frac{c_f}{2H}\bar{u}\sqrt{\bar{u}^2 + \bar{v}^2} + \nu_t\left(\frac{\partial^2 \bar{u}}{\partial x^2} + \frac{\partial^2 \bar{u}}{\partial y^2}\right), \tag{9}$$

$$\frac{\partial \bar{v}}{\partial t} + \bar{u}\frac{\partial \bar{v}}{\partial x} + \bar{v}\frac{\partial \bar{v}}{\partial y} = -\frac{\partial \bar{p}}{\partial y} - \frac{c_f}{2H}\bar{v}\sqrt{\bar{u}^2 + \bar{v}^2} + \nu_t\left(\frac{\partial^2 \bar{v}}{\partial x^2} + \frac{\partial^2 \bar{v}}{\partial y^2}\right). \tag{10}$$

where the overbar denotes depth-averaged quantities and c_f is the friction coefficient. The effect of sub-depth motion on the depth averaged flow field, which emerges because of the non-uniformity of the veclocity field with respect to depth, is lumped into the eddy viscosity terms as in [30] and ν_t is eddy viscosity.

2.2 Reduced dimensionality model for a shallow flow with important Froude number effects

As the Froude number increases, the vertical velocity at the free-surface may not be negligible. The hydrostatic pressure distribution emerges from the shallowness assumption $H/L \ll 1$ together with Eq. (4). Integrating the mass and horizontal momentum equations vertically and combining with the kinematic free surface condition and the boundary conditions at the bed lead to the classical shallow water equations (see e.g. [74]):

$$\frac{\partial \bar{u}}{\partial t} + \bar{u}\frac{\partial \bar{u}}{\partial x} + \bar{v}\frac{\partial \bar{u}}{\partial y} = -g\frac{\partial h}{\partial x} - \frac{c_f}{2h}\bar{u}\sqrt{\bar{u}^2 + \bar{v}^2} + \nu_t\left(\frac{\partial^2 \bar{u}}{\partial x^2} + \frac{\partial^2 \bar{u}}{\partial y^2}\right), \tag{11}$$

$$\frac{\partial \bar{v}}{\partial t} + \bar{u}\frac{\partial \bar{v}}{\partial x} + \bar{v}\frac{\partial \bar{v}}{\partial y} = -g\frac{\partial h}{\partial y} - \frac{c_f}{2h}\bar{v}\sqrt{\bar{u}^2 + \bar{v}^2} + \nu_t\left(\frac{\partial^2 \bar{v}}{\partial x^2} + \frac{\partial^2 \bar{v}}{\partial y^2}\right), \tag{12}$$

$$\frac{\partial h}{\partial t} + \frac{\partial}{\partial x}(\bar{u}h) + \frac{\partial}{\partial y}(\bar{v}h) = 0, \tag{13}$$

where h is water depth. For convenience, the overbar is dropped from here onwards.

While reduced dimensionality models capture key physics in shallow shear flows, water quality predictions in such flows require three-dimensional models due to the presence of secondary circulations and other three-dimensional effects [1, 2, 7].

3 Hydrodynamic stability theory

The onset and growth of 2DCS in shallow shear flows have been explained under the context of hydrodynamic stability theory [25, 36, 45]. Hydrodynamic stability theory is a branch of fluid mechanics that explains the transition from laminar to turbulent flows. Perturbations always exist in any real flow. In the framework of linear stability theory it is assumed that perturbations are small. Under certain conditions, the perturbations can grow and reach at some time sufficiently large amplitude to change the base flow. The base flow is said to be unstable under such conditions. As a result of instability of the base flow one can observe either a laminar flow with more complicated structures (as in the case of Taylor–Couette flow between two rotating cylinders) or rapid transition to turbulence (as in the case of a pipe Poiseuille flow). Considering spatially developing flows, e.g. mixing layers and wakes, the base flow is not uniform in the streamwise direction. However, in most of such flows streamwise variations of the mean flow are slow over a typical instability wavelength. It is thus reasonable to consider a local velocity profile at a particular (usually upstream) station under the assumption that this profile stays self-similar for all stations downstream (parallel flow assumption). If a localized disturbance (or mode) is growing while travelling in the flow domain, the base flow becomes unstable. There are two different scenarios of the behavior of the unstable perturbation. If the growing perturbation is eventually convected away and leaves the flow domain the flow is said to be convectively unstable. On the other hand, if the unstable perturbation occupies the whole domain the flow is said to be absolutely unstable. Figure 1 illustrates the concept of absolute/

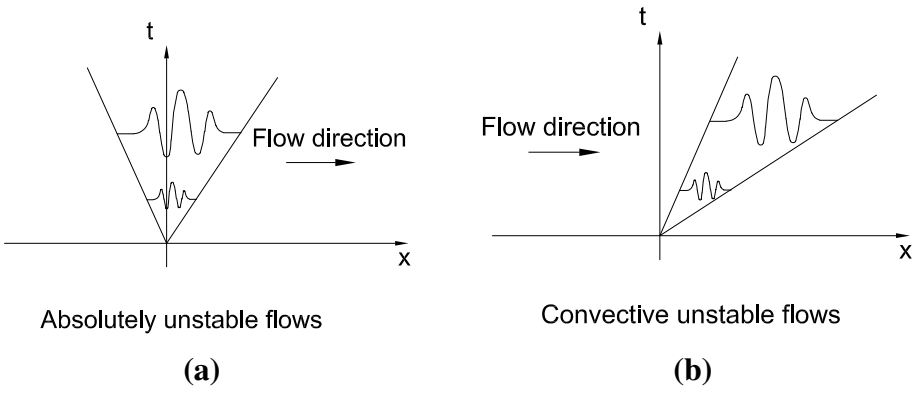

Fig. 1 Perturbation dynamics of absolutely unstable flow (**a**); and convective unstable flow (**b**). Note that in **a** the perturbation grows and spreads both upstream and downstream; in **b** the perturbation grows but is washed to the downstream

convective instability. These concepts were introduced by Bers [6] and readers can also see [33] for a review.

Hydrodynamic stability theory is successful for free shear flows, e.g. mixing layers [32], wakes [62]. For shallow shear flows, the bed friction turbulence can be simplified as an eddy viscosity and a quadratic bed friction terms by the virtue of scale separation. Two-dimensional stability theory is thus invoked to investigate the onset of 2DCS. The approach has some success in characterizing flow stability and explaining the size and amplitude of 2DCS [3, 11, 16, 72]. Attempts have also been made to associate different flow regimes in shallow wakes in experiments (see, for example, [10]) with absolute and convective instabilities. As the ratio of the dissipative force to the driving force decreases, three different flow patterns are identified experimentally: Steady Bubble (SB), Unsteady Bubble (UB), and Vortex Street (VS). From a linear stability point of view the transition from SB to UB represents the transition from linearly stable to linearly unstable flow. Attempts to describe the transition from UB to VS using concepts of absolute and convective instabilities are made in [11, 25, 45] with a certain success. In particular, the transition from UB to VS is associated with the transition from convective to absolute instability. This section introduces several stability theories and their relevance to shallow flows.

3.1 Linear stability theory

To determine the stability characteristics of a flow, linear stability analysis is invoked. The method is described as follows: (1) define a base flow; (2) linearize the equations of motion in the neighborhood of the base flow; (3) solve the linearized eigenvalue problem and find the critical values of the parameters and the region of linear stability and instability; (4) analyze the development of perturbations in unstable region. Base flow in the analysis is obtained as a steady one-dimensional solution of the equations of motion. Assuming that the flow is moving in the x-direction it would be natural to follow the classical theory and assume that the base flow velocity vector has the form

$$\mathbf{v} = (U(y), 0). \tag{14}$$

Substituting (14) into (8), (9), (10) we obtain

$$\frac{\partial p}{\partial x} + \frac{c_f}{2H} U^2(y) = 0, \quad \frac{\partial p}{\partial y} = 0. \tag{15}$$

Solution of equation 15 is $U(y) = U_0$ where U_0 is a constant, which is not interesting since the velocity gradient is the crux for shear instability. There are several ways to overcome this difficulty. Additional empirical parameters (such as eddy viscosity) can be used to derive the base flows velocity distribution. This approach is used, for example, in [52, 65] for mixing layer flows generated by vegetation. Asymptotic expansions for two dimensional laminar wake flows are obtained in [5, 68]. Finally, model base flow profiles (such as a hyperbolic tangent profile for mixing layers or a hyperbolic secant profile for wakes) which resemble the velocity distribution obtained in experiments are also widely used in practice. This approach is used, for example, in [10–13, 23, 25, 44, 45, 72].

Consider a perturbed solution of the system (8),(9),(10) of the form

$$u(x, y, t) = U(y) + u'(x, y, t), \quad v(x, y, t) = v'(x, y, t), \quad p(x, y, t) = P(x) + p'(x, y, t), \tag{16}$$

where the quantities with primes represent small unsteady perturbations. Substituting (16) into (8),(9) and (10), linearizing the resulting system in the neighborhood of the base flow, eliminating the pressure perturbation, introducing the stream function by the relations

$$u' = \frac{\partial \psi'}{\partial y}, \quad v' = -\frac{\partial \psi'}{\partial x} \tag{17}$$

and dropping the primes we obtain the linearized equation for the perturbation of the stream function in the form

$$\begin{aligned} &\psi_{xxt} + \psi_{yyt} + \psi_{0y}(\psi_{xxx} + \psi_{xyy}) - \psi_{0yyy}\psi_x \\ &\frac{c_f}{2H}(\psi_{0y}\psi_{xx} + 2\psi_{0yy}\psi_y + 2\psi_{0y}\psi_{yy}) = 0, \end{aligned} \tag{18}$$

where the subscripts indicate the partial derivatives with respect to the independent variables.

The method of normal modes is used next to analyze the linear stability of the base flow (see, for example, [20]). The perturbation of the stream function is assumed to be of the form

$$\psi(x, y, t) = \varphi(y)\, e^{ik(x-ct)}, \tag{19}$$

where $\varphi(y)$ is the amplitude of the normal perturbation, k is the wave number and c is the phase speed of the perturbation. Substituting (19) into (18) we obtain

$$(U - c)k\varphi'' - iSU\varphi' - iSU_y\varphi' + (k^3(c - U) - kU_{yy} + ikSU/2)\varphi = 0, \tag{20}$$

where $S = c_f b/H$ is the bed friction number and b is the lengthscale of the transverse shear layer. The boundary conditions are (assuming that fluid layer is infinite in the transverse direction):

$$\varphi(\pm\infty) = 0. \tag{21}$$

Problem (20), (21) is an eigenvalue problem. Thus, for a fixed S a nontrivial solution of (20), (21) exists only for certain values of the parameters k and c.

Problem (20) and (21) can be solved with a chosen $U(y)$ numerically using a collocation method based on the Chebyshev polynomials (see, for example, [23] for details). There are two approaches to the solution of the eigenvalue problem (20) and (21): (a) temporal stability analysis and (b) spatial stability analysis. In the temporal case we assume that the wave number k is real while the phase speed c is complex: $c = c_r + ic_i$. As can be seen from Eq. (20), the corresponding eigenvalue problem is linear with respect to c. As a result, a generalized eigenvalue problem obtained after discretization of Eq. (20) is linear in c and can be solved using standard routines, say, in Matlab. The base flow is linearly stable if all c_i are negative and linearly unstable if at least one $c_i > 0$. For the given base flow a marginal stability curve in the (k, S)-plane corresponds to the case $c_i = 0$ and separates the regions of stability and instability of the base flow. In the spatial case the parameter c is assumed to be real while the wave number k is complex: $k = k_r + ik_i$. The base flow is linearly stable if all $k_i > 0$ and linearly unstable if at least one $k_i < 0$. The corresponding eigenvalue problem (20), (21) is nonlinear in k. Thus, from a computational point of view it is more difficult to solve the spatial stability problem. In order to overcome this difficulty in a vicinity of a marginal stability curve a transformation is proposed (see [22]) which allow one to calculate spatial growth rates if temporal growth rates are known. However, such a transformation is valid only in a small neighborhood of the marginal stability curve

(in other words, it is applicable only for small spatial and temporal growth rates). This fact is supported by linear stability calculations in [26]. The absolute/convective stability characteristics of the flow can also be determined by solving (20) and (21) with both k and c are complex. The solution for complex k and c is sought by a saddle point search technique [27].

3.2 Weakly nonlinear analysis

Linear stability theory can answer the following questions: (1) When does a particular base flow become unstable? (2) What are the critical values of the parameters at the stability boundary (wave number, wave speed, bed friction number)? The "fate" of unstable perturbation above the threshold cannot be predicted by linear stability theory. Assuming that the bed friction number S is slightly smaller than the critical value S_c (in other words, assuming that the growth rate of the unstable perturbation is small) one can apply weakly nonlinear theory in an attempt to analyze the development of instability (at least at the initial stage). The perturbed stream function in (19) is modified by introducing an unknown amplitude function $A(\xi, \tau)$:

$$\psi(x, y, t, \xi, \tau) = A(\xi, \tau)\varphi(y)\, e^{ik(x-ct)}, \tag{22}$$

where $\xi = \varepsilon(x - c_g t)$ and $\tau = \varepsilon^2 t$ are the "slow" longitudinal coordinate and time, respectively, and c_g is the group velocity. The idea of using the method of multiple scales comes from the fact that the amplitude A varies slowly in comparison with the change of the phase of the unstable perturbation. Such an approach is used, for example, in [45] for the analysis of wake flows. Expanding the stream function in powers of ε, using solvability conditions (see [45]) and rescaling the amplitude function we obtain the complex Ginzburg–Landau equation of the form

$$\frac{\partial A}{\partial \tau} = A + (1 + c_1 i)\frac{\partial^2 A}{\partial \xi^2} - (1 + c_2 i)|A|^2 A, \tag{23}$$

where the values of the real coefficients c_1 and c_2 are obtained in closed form in terms of integrals containing the characteristics of the linearized problems. It is shown in [45] that Eq. (23) can be used to explain some characteristics of shallow wake flows (see Sect. 4).

3.3 Nonlinear mean-field theory

While the weakly nonlinear Ginzburg–Landau equation is suitable for $S \to S_c$ [8, 45], the equation may not be applicable under $S \ll S_c$ where S_c is the critical value of S from the linear theory. In this case, the mean field theory provides a promising alternative. In physics, mean field theory refers to the use of a mean field to represent the interaction of a molecule with its neighbor molecules instead of modeling every interaction between the molecule and all its neighbors. Similarly, in stability analysis, the interaction between the mode of interest and the mean field rather than the interactions of this mode with every other mode is represented [4, 54]. One example is the interaction between the fundamental mode and the mean flow field via Reynolds stresses. The interaction distorts the mean flow field and this distortion becomes more significant as the Reynolds stress of the fundamental mode becomes sufficiently large. This distortion changes the base flow field and thus its stability characteristics. For example, for base flows that are linearly unstable, the distortion of the mean flow may cause a decrease in the growth of the fundamental mode by the

mean flow. When the production of the fundamental mode energy decreases to an extent that the magnitude of the production is similar to other dissipative mechanisms, a finite amplitude equilibrium state is reached. The interaction between the fundamental mode and the mean flow field can in some cases be destabilizing. For example, linear stability calculations show that pipe Poiseuille velocity profile is linearly stable for all Reynolds numbers while the critical values of the Reynolds number for plane Poiseuille flow are much larger than the corresponding experimental values. On the other hand, mean field theory has been successful in showing that the distortion of the mean base flow renders the flow unstable for finite and realistic Reynolds numbers ($Re = 2500-3000$ [28, 55]). The results of the mean field theory for shallow mixing layers are presented in Sect. 5 of this paper.

3.4 Secondary linear stability theory

Secondary linear stability theory investigates if the coherent structures that result from the primary instability are themselves unstable to small perturbations. Such theory has been instrumental in deep mixing layers (e.g., [56, 61]). Kelly [40] investigated the stability of a base flow comprised of the most unstable mode superimposed on a hyperbolic tangent velocity profile and found good consistency between theory and experiments. Pierrehumbert and Widnall [61] added complexity to the secondary stability analysis in Kelly [40] by choosing the base flow to be the Stuart vortex. The Stuart vortex is the exact solution of the two dimensional Euler equations discovered by Stuart [67] representing fully developed coherent structures in deep mixing layers. Pierrehumbert and Widnall [61] showed that the Stuart vortex is unstable to a perturbation with a wavelength double the length of a Stuart vortex. Vortex merging occurs as the result of instability. Metcalfe et al. [56] tested the secondary instability of coherent structures in deep mixing layers with direct numerical integration of the flow equations. The subharmonic perturbations added onto the coherent structures were shown able to trigger the pairing of the coherent structures. Klaassen and Peltier [42] showed that there are two instability modes in viscous, moderately stratified Stuart vortex; they are namely (1) the orbital mode; and (2) the draining mode. The orbital mode advects the coherent structures up and down in an alternate manner, which is consistent with the vortex pairing motion observed in deep mixing layers (e.g. [31, 58]). The draining mode strengthens and weakens the coherent structures in an alternate manner, which is consistent with the vortex shredding of coherent structures in stratified and unstratified deep mixing layers simulated in Patnaik et al. [58] and Riley and Metcalfe [63]. In shallow flows, the results in Ghidaoui et al. [25] indicate the presence of secondary instability in vortex shedding and unsteady bubble flows. The use of secondary linear stability theory in shallow mixing layers is illustrated in Sect. 5.

4 Application 1: Shallow wakes

Figure 2 shows the vorticity contours of numerically simulated shallow wakes in the lee of cylindrical bluff bodies in [25]. Figure 2a shows that when $S = 0.17$, the cylinder wake is characterized by a pronounced vortex shedding mechanism, leading to the establishment of a vortex street pattern. Figure 2b shows the cylinder wake for $S = 0.35$. An unsteady bubble, characterized by a re-circulating flow region, emerges in the near wake of the cylinder. Downstream of the unsteady bubbles, a sinuous wake is observed. For both flow regimes, vortices shed from the cylinder at frequencies referred to as the shedding frequencies.

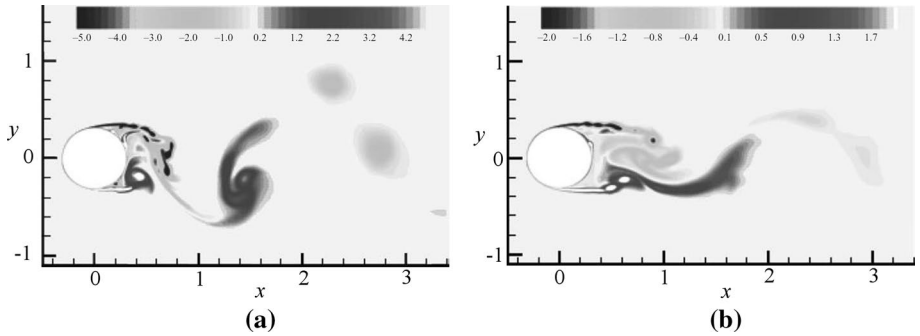

Fig. 2 Shallow wake flow patterns. Vortex shedding (VS), S = 0.17 (**a**); unsteady bubble (UB), S = 0.35 (**b**). From *Journal of Fluid Mechanics*[25]. Reprint with permission

Further increase in S (> 0.5) results in a steady bubble flow in which the flow ceases to oscillate.

The results of linear and weakly nonlinear theories are compared to the results of nonlinear simulations in [29] ([45, 25]). First, the critical values of the local (i.e. at a particular downstream location of the flows) stability parameter S are in good agreement—numerical model predicts $S_c = 0.2$ (beyond which the flow is in SB regime) while linear stability theory (temporal analysis) gives $S_c = 0.196$. Second, the real part of the constant in front of the term $|A|^2A$ in nonscaled Ginzburg–Landau equation is negative (thus, a finite amplitude saturation is possible, Fig. 3). Third, the saturation amplitude of the unstable perturbation in a convectively unstable region is predicted reasonably well by the weakly nonlinear theory. It is shown in [29] that for $S = 0.14$ the saturation amplitude A is about 0.14. Under some simplifying assumptions (along-stream evolution as $\xi \to \infty$ and $\tau \to \infty$) the Ginzburg–Landau equation gives $A = 0.13$ for the case $S = 0.196$. Thus, the results of weakly nonlinear model compare reasonably well with numerical simulations in [29]. Fourth, it is shown in [25] that the Benjamin–Feir instability condition

$$1 + c_1 c_2 < 0 \tag{24}$$

is satisfied for shallow wake flows. This condition implies that plane wave solutions of (23) are unstable (and, therefore, are not observable in experiments). This fact is supported by experimental data in [11].

Absolute and convective instability analyses are used in [25] to establish a link between the shedding frequency and the characteristics of the absolute and convectively unstable flows. It is shown, in particular, that in the VS regime the criterion proposed by Koch [43] compares well with nonlinear simulations: the global frequency of oscillations (the

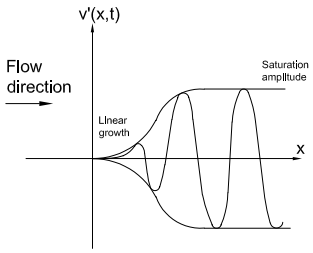

Fig. 3 Perturbation dynamics described by the Ginzburg–Landau equation. For a linearly unstable flow, the perturbations grow at the upstream. When the perturbation amplitude becomes non-negligible, nonlinearity reduces the perturbation growth rate, causing the perturbation amplitude to saturate

Strouhal number) from the nonlinear simulations is $St = 0.217$ while the local frequency of oscillations calculated at the transition point from convective to absolute instabilities is $St = 0.208$. Good match between the two results can be partially explained by the fact that the base flow profile in [25] is the time-averaged flow in the VS regime. On the other hand, the comparison based on the Koch criterion gives rather poor results in the UB case. However, the criterion proposed in [59, 60] compares better to the results from nonlinear simulations. Thus, the wave-maker mechanism proposed in [59, 60] seems to be valid also for shallow flows. The proposed mechanism is based on the assumption that the perturbations pile up at the location x_{ca}, where the transition from convective to absolute instability takes place. This process triggers the VS motion at the frequency which is equal to the frequency obtained from the linear analysis at x_{ca}.

In many linear stability analyses of shallow wake flows with bottom friction the base flow is represented by model velocity profiles obtained either from experiments or from time-averaged velocity profiles from numerical simulations. The wake generating obstacle is not taken into account in this case. It is shown in [9] that the structure of wake flow remains similar in both cases: (a) when the actual obstacle is present and (b) when the obstacle is absent. Thus, such an analysis supports the use of model velocity profiles in linear stability analysis of shallow wake flows.

5 Application 2: Shallow mixing layers

The onset and development of 2DCS in shallow mixing layers depends also on the ratio between friction and horizontal velocity shear. However, there are two velocity scales in a mixing layer, the velocity difference between the two streams ΔU and the average velocity of the two streams $\overline{U}$ respectively. Thus the stability parameter is defined as $S = \frac{c_f \delta}{2H} \frac{\overline{U}}{\Delta U}$ where δ is the mixing layer thickness. Figure 4 displays the vorticity field of a shallow mixing layer, illustrating the spatial development of flow instability. From the inflow boundary and to about $x = 2.0$ m, the perturbation is small and wavy, but spatially growing if $S < S_c$. In the region from about $x = 2.0$ m to about 3.0 m, the perturbation changes from wavy to large scale vortical structures. From about $x = 3.0$ m to about 12.0 m, the vortical structures merge with other structures, forming larger vortical structures. Within this region, from $x = 3.0$ to 5.0 m, the vortices experience slight lateral displacement and the mechanism of vortex induction commences. The process of first vortex merging appears to begin around $x = 5.0$ m and is complete around $x = 9.0$ m. The second vortex merging takes place in the region $x = 9.0$ m to about $x = 12.0$ m. Beyond $x = 12.0$ m, the mechanism of vortex merging appears to become suppressed. In fact, a reduction in strength of the large scale vortices is clearly seen in Fig. 4 just after $x = 14$ m.

Shallow mixing layers are convectively unstable flows [66]; the perturbations are usually considered to be subjected to the instability of local base flows as the perturbations

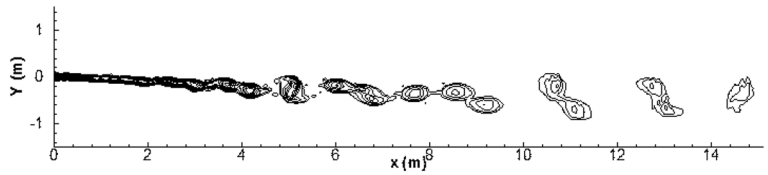

Fig. 4 Numerically simulated shallow mixing layer Adopted from Liang [51]

are convected downstream. Chu and Babarutsi [15] chose the base flow to be the local parallel mean velocity profiles implicitly by suggesting the stability parameter S varies with downstream position x. At a location where $S(x) = S_c$, perturbations cease to grow and the flow is stable downstream of the location. van Prooijen and Uijttewaal [72] conducted linear stability analysis explicitly with the local parallel mean velocity profiles being the base flow. The upstream growth and cessation of growth at certain downstream locations in their experiments were successfully reproduced. However, the success is attributed to the fact that nonlinear effects are accounted for in the mean velocity profile used a base flow. The approach of using base flows derived from experiments or nonlinear models in linear analysis more likely to rediscover the flow dynamics from which they were derived than to explain the underlying instability. Lam et al. [49] sought a fundamental explanation to the onset, formation and growth of 2DCS by using a sequence of stability theories, namely the linear theory, nonlinear mean field theory and secondary stability theory, in the context of convectively unstable flows [18].

5.1 The linear region

At the upstream (or linear region) of the mixing layer, perturbations are selectively amplified. To illustrate the idea, linear stability analysis of shallow mixing layers is conducted. Suppose that the velocities of undisturbed flow are U_1 and U_2 at $y = -\infty$ and $y = \infty$, respectively. The base flow velocity profile $U(y)$ is chosen to be in the form [72]

$$U(y) = \frac{U_2 + U_1}{2} + \frac{U_2 - U_1}{2} \tanh(\gamma y), \tag{25}$$

where γ is the parameter characterizing the lengthscale of the velocity gradient. Choosing the velocity scale of the form $(U_2 - U_1)/2$ we rewrite (25) in the dimensionless form

$$U(y) = B + \tanh(\gamma y), \tag{26}$$

where $B = (U_2 + U_1)/(U_2 - U_1)$ is the velocity ratio.

A sample calculation of the marginal stability curve for the case $B = 2$ is shown in Fig. 5. The region of instability is above the curve. The bed friction parameter required for stabilization depends on the wavenumber k of the modes. The maximum point on the marginal stability curve defines the critical values of the parameters of the problem; $S = S_c$ is the critical stability parameter; $k = k_c$ and $c_r = c_c$ are wavenumber and phase speed of the most unstable mode. The analysis here gives $S_c \sim 0.1$, which agrees with the transition between stable and unstable flow in experiments [15, 69]. The modal turbulent energy obtained from the linear stability analysis also agrees with experiments [72].

5.2 Beyond the linear region

The relevance of stability theories in shallow mixing layers beyond the linear region is illustrated by numerical simulations with hydraulic parameters of the experiment case 42 in [72]. The experiment was conducted in a shallow flow facility in the Delft University of Technology. Two incoming flows, $U_1 = 0.11$ m/s and $U_2 = 0.25$ m/s respectively, came into contact. The water depth was 0.042 m and $c_f = 0.0064$. The mixing layer thickness was estimated to be $\delta = 0.05$ m at a location where the two streams start coming into contact. The simulation is conducted in a moving frame of reference. The velocity of the frame of reference is that of the inflexion point of the mixing layer velocity profile $\overline{U}$. The

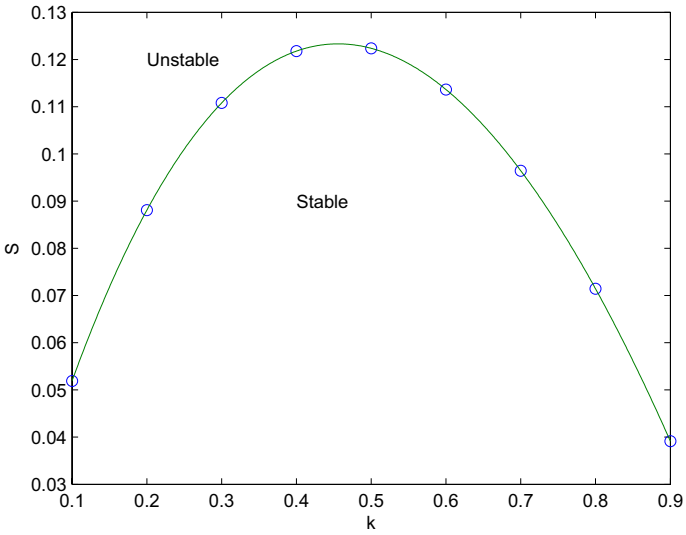

Fig. 5 Marginal stability curve for shallow mixing layers

resulting Galilean transformed shallow water equations are solved numerically by the Boltzmann–Gross–Krook (BGK) finite-volume scheme [24]. The periodic boundary conditions are used in streamwise boundaries, and the transmissive (zero-gradient) boundary conditions are used in spanwise boundaries. The initial base velocity profile $U(y, t = 0)$ is

$$U(x, y, t = 0) = \frac{\Delta U_0}{2} \tanh\left(\frac{2y}{\delta_0}\right) \tag{27}$$

with $\Delta U_0 = U_2 - U_1$ being the initial velocity difference between the fast and slow streams and $\delta_0 = 2/\gamma$ being the initial mixing layer thickness. Two numerical simulations, both perturbed with the fundamental and the subharmonic modes of equal energy, are conducted. In one of the simulations, the phase angle difference between the fundamental and subharmonic modes is zero. The simulation is referred to as "Simulation 2–0"; "2" means the flow is perturbed with mainly two modes; "0" means the phase angle difference is zero. In the other simulation, the phase angle difference is $\pi/2$. The simulation is referred to as "Simulation 2-$\pi/2$". Readers are referred to [48] for the details of the simulations.

Figure 6a shows that the initial condition is in the form of a perturbed vortex line which is susceptible to KH instability in all simulations (only simulation 2–0 is shown here). The modal growth rate agrees with the linear theory up to $\overline{U}t = 0.3$ m. While the perturbation amplitude becomes sufficiently large, nonlinear self-interaction of the fundamental mode causes the change of flow structure from a plane wave type to fully developed 2DCS as shown in Fig. 6b. Such change is consistent with the change in the flow field of the fundamental mode in the mean-field theory, which is discussed in Sect. 5.2.1. Beyond the full formation of 2DCS, such structures merge to form larger ones. However, the 2DCS merging mechanism is sensitive to the phase-angle difference. 2DCS in simulation 2–0 merge via the pairing mechanism. In this mechanism, the 2DCS arrange in pairs and the 2DCS in each pair twist around one another for some time then merge into larger 2DCS. In simulation 2-$\pi/2$, the 2DCS merge via the shredding of 2DCS. In this mechanism, each of the weaker 2DCS is located between two

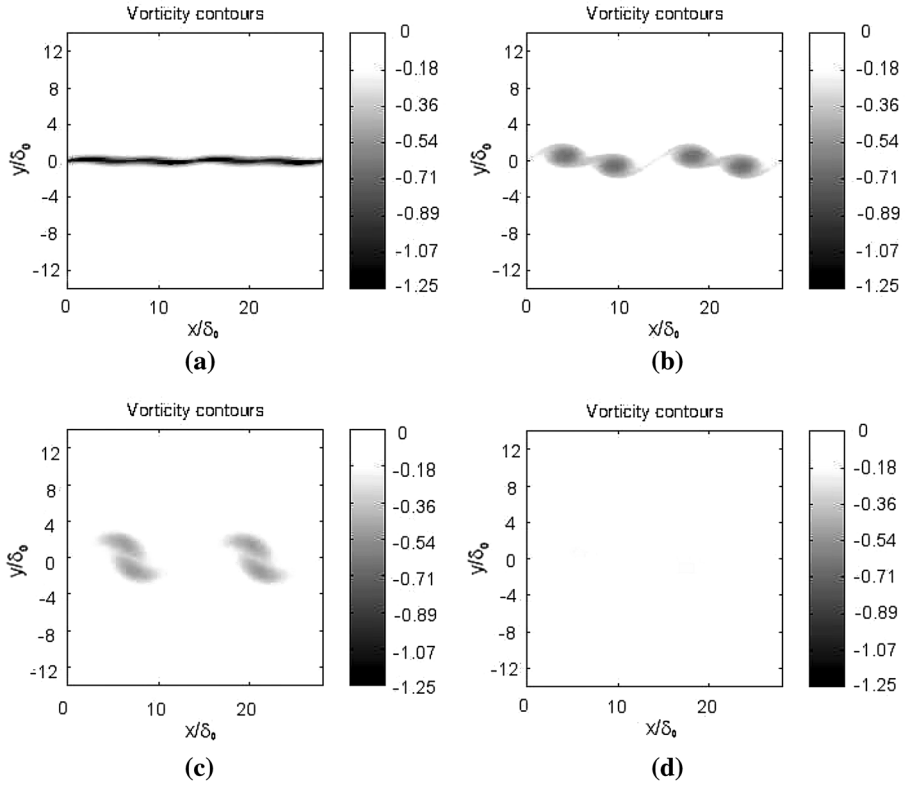

Fig. 6 The vorticity contours for simulation 2–0 at $\overline{U}t = 0$ m (**a**), $\overline{U}t = 1.03$ m (**b**), $\overline{U}t = 1.93$ m (**c**) and $\overline{U}t = 7.49$ m (**d**)

stronger 2DCS and vice versa. The weaker 2DCS are then deformed in the flow fields of the stronger 2DCS as shown in Fig. 7. The vorticity of the weaker 2DCS is then absorbed into the stronger 2DCS. The merging of 2DCS is a consequence of secondary instability of the 2DCS. The idea is further discussed in Sect. 5.2.2.

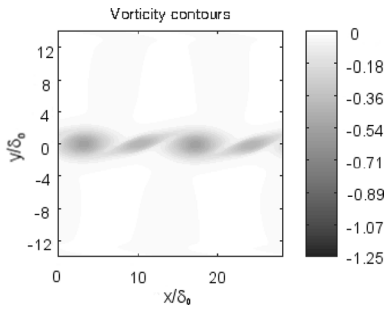

Fig. 7 The vorticity contours for simulation 2-π/2 at $\overline{U}t = 1.93$ m

5.2.1 Analysis for mean-field theory

To illustrate correspondence between the roll-up of 2DCS and the mean-field theory, an initial value problem (IVP) that accounts for the interactions between the mean flow, the fundamental mode and the first harmonic mode is formulated in a frame of reference moving with the coherent structures. Considering flows with low Froude numbers, the rigid-lid assumption is applied. The equations are further decomposed into Fourier modes where only the mean flow field, the fundamental mode, the first harmonic mode and their interaction are retained. The result is an initial value problem (IVP) and is referred to as "2-mode-mean-field". For comparison, another IVP is formed with the first harmonic mode also removed from the Fourier decomposed shallow water equations. This IVP is referred to as "1-mode-mean-field". The solution scheme for the IVPs is described in [48]. The IVP uses the eigenfunctions obtained from linear stability analysis as the initial conditions. This is different from the dynamical system approach which relies on proper orthogonal decomposition (POD) to determine the basis function from experiments or numerical results.

The IVP is solved for the flow case 42 in [71]. Figure 8 shows the development of the fundamental mode in "1-mode-mean-field" during the formation of 2DCS. The flow field gives a large modal energy production at the centerline of the mixing layer because of its large $-u'v'$ at the centerline. As the fundamental mode grows, the flow field of the fundamental mode changes in shape, resulting in smaller modal energy production. When the flow field of the fundamental mode further changes such that the modal energy production

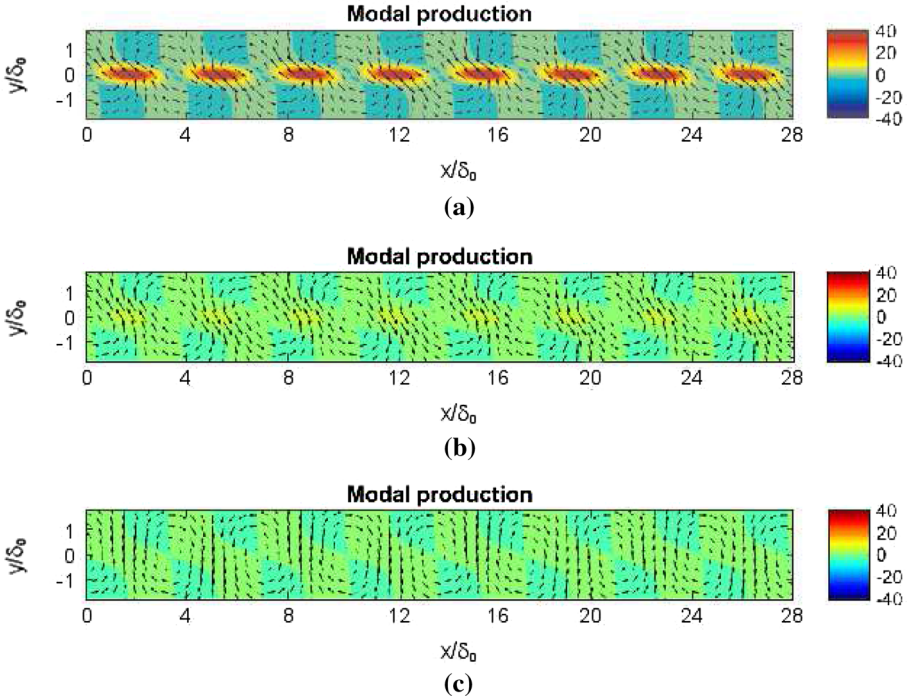

Fig. 8 The velocity field (vectors) and the normalized production (color contour) of the fundamental modal energy in "1-mode-mean-field" at $\overline{U}t = 0$ m (**a**), $\overline{U}t = 0.54$ m (**b**) and $\overline{U}t = 1.09$ m (**c**)

is balanced by other dissipative mechanisms, namely eddy viscosity and bed friction, the flow reaches a finite-amplitude equilibrium state. This is consistent with the change of flow structure from a plane wave type to fully developed 2DCS in numerical simulations.

5.2.2 Secondary stability analysis

As for shallow wakes (see Sect. 4), the coherent structures are susceptible to secondary instability if the Benjamin–Feir instability condition is satisfied. Indeed, such a criteria is satisfied for the problem under consideration. Therefore, secondary stability analysis can be conducted by using the Stuart vortex (Fig. 9) as the base flow. The Stuart vortex is the exact solution of the two-dimensional Euler equations derived by [67], which reads

$$U^s(x,y) = \frac{(\triangle U^s/2)\sinh\left(\frac{2\pi y}{L}\right)}{\left(\cosh\left(\frac{2\pi y}{L}\right) + a\cos\left(\frac{2\pi x}{L}\right)\right)} \tag{28}$$

$$V^s(x,y) = \frac{a\left(\triangle U^s/2\right)\sin\left(\frac{2\pi x}{L}\right)}{\left(\cosh\left(\frac{2\pi y}{L}\right) + a\cos\left(\frac{2\pi x}{L}\right)\right)} \tag{29}$$

Here $U^s(x,y)$, $V^s(x,y)$ are the streamwise and cross-stream velocities of the Stuart vortex; ΔU^s is the velocity difference across the Stuart vortex; L is the vortex size. The base flow should be chosen at the finite amplitude equilibrium (i.e. full formation of 2DCS) where the 2DCS themselves do not change rapidly.

Similar to the primary linear stability analysis, the method of normal modes is applied to the secondary linear stability analysis. For a periodic base flow, Floquet theory suggests that the form of solutions for the perturbed flow quantities should be chosen as [42, 64]

$$\begin{pmatrix} h' \\ u' \\ v' \end{pmatrix} = \begin{pmatrix} \hat{\hat{h}}_\alpha(x,y) \\ \hat{\hat{u}}_\alpha(x,y) \\ \hat{\hat{v}}_\alpha(x,y) \end{pmatrix} e^{i\alpha x} e^{\sigma t} \tag{30}$$

where α is the Floquet parameter; $\sigma = \sigma_r + i\sigma_i$ is a complex growth rate; and $\hat{\hat{u}}_\alpha$, $\hat{\hat{v}}_\alpha$ and $\hat{\hat{h}}_\alpha$ are periodic functions in x with period equals to the one in the base flow. The governing equations are then linearized and are solved as an eigenvalue problem with a pseudo-spectral collocation method.

Figure 10 shows the growth rate of the pairing mode and the shredding mode. As expected from the observed pairing of two 2DCS into a larger coherent structure in shallow mixing layers [51] and shallow jets [19], the most unstable Floquet parameter for both the pairing and shredding modes is $\alpha/k_{fun} = 0.5$, corresponding to the dimensional wavenumber of the subharmonic mode ($k = 2$). The presence of two modes of instability and the fact that the most unstable mode is at the subharmonic wavenumber is consistent with the numerical simulations.

Further research can be directed to answer the questions below with three-dimensional numerical simulations; (1) validity of the hydrodynamic stability theories; and (2) the

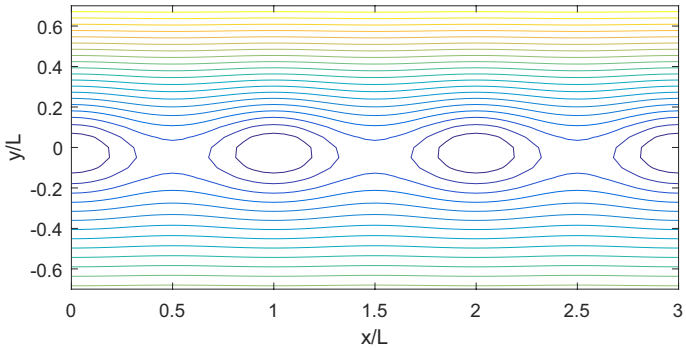

Fig. 9 The streamfunction of Stuart vortex

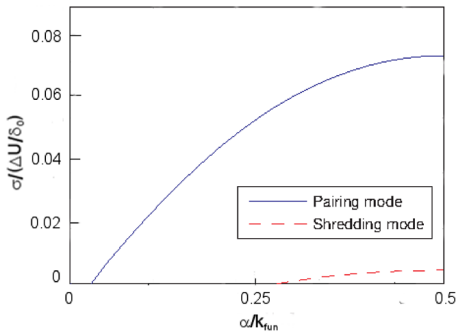

Fig. 10 Growth rate versus Floquet parameter α for the secondary instability of the Stuart vortex

respective roles of hydrodynamic stability theories and inverse energy cascade in 2DCS development.

6 Application 3: Froude number effect

Shallow shear flows with low Froude numbers are discussed in Sects. 4 and 5. With higher Froude numbers, the effect of gravity wave on shear instability needs consideration. Gravity waves are known to stabilize the flow, but such stabilizing effect is only obvious under higher Froude numbers ($Fr > 0.6$). Numerical study of longshore currents in [21] and linear stability analysis in [23] show that the stabilizing effect of gravity waves is not important when $Fr < 0.6$. Linear stability analysis of shallow wakes in [45] shows that the difference in S_c between linear stability analyses with and without gravity wave effect is less than 10% when $Fr < 0.6$. However, since the velocity gradients govern the formation of 2DCS, the convective Froude number ($Fr_c = \Delta U/(2\sqrt{gH})$) is a more appropriate parameter, where ΔU is the velocity difference across the shallow layer [38, 39]. In a shallow mixing layer with high Fr_c, gravity waves emanate from the coherent structures in the form of shock waves. Part of the energy in the shear layer is radiated with the waves, leaving less energy for the KH instability. The result is that gravity waves play a stabilizing effect on shallow shear flows [14].

To illustrate the effect of gravity waves, numerical simulations with temporal shallow mixing layers with $Fr_c = 0.4$ and $Fr_c = 1.2$ are conducted. A natural choice of initial perturbations for the simulations $Fr_c = 0.4$ and $Fr_c = 1.2$ are their respective most amplified modes obtained from linear stability analysis without the rigid-lid assumption. However, the resulting eigenfunctions for the two cases are different. Linear and nonlinear growth simulated with such initial conditions shows only the combined effect of the flow dynamics and the difference in initial conditions. To isolated the effect of the dynamics from the difference in initial conditions, the initial perturbation used here for both $Fr_c = 0.4$ and $Fr_c = 1.2$ simulations is the superposition of the most amplified eigenfunctions of the fundamental and subharmonic modes for incompressible mixing layers obtained from linear stability analysis with the rigid-lid assumption.

Table 1 shows the initial modal growth of the fundamental and subharmonic modes, the time at which the fundamental modal energy is at its peak (t_p^*), and the energy amplification at t_p^*. Figure 11 shows the water depth and vorticity for $Fr_c = 0.4$ and $Fr_c = 1.2$ respectively. At the start, the modal growth rate in the two simulations agree well with the linear stability results. This is expected as the initial amplitude and form of perturbations in the simulations are obtained from the eigenfunctions of the linear stability

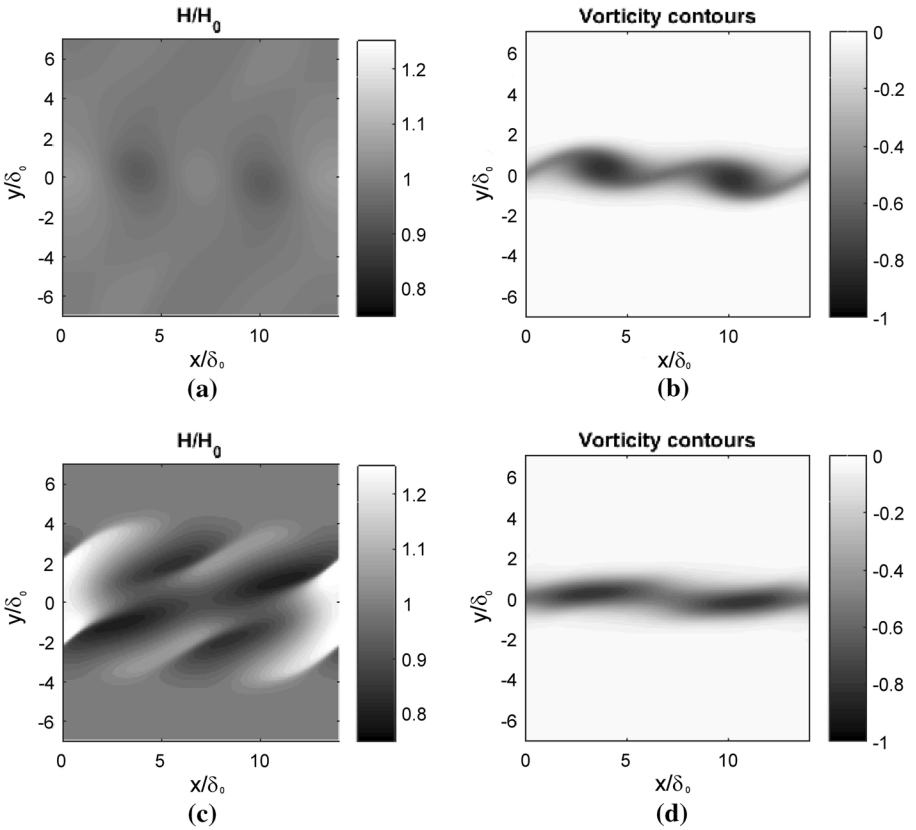

Fig. 11 **a** Water depth and **b** Vorticity contours of numerical simulation with $Fr_c = 0.4$ at $t = 9\delta_0/\Delta U$; **c** water depth and **d** Vorticity contours of numerical simulation with $Fr_c = 1.2$ at $t = 9\delta_0/\Delta U$

Table 1 Initial dimensionless growth rate of the fundamental mode (σ^*_{fun}) and subharmonic modes (σ^*_{sub}), the time when fundamental energy reaches its peak (t^*_p) and the amplification of energy at t^*_p ($E_{fun,t_p}/E_{fun,0}$). The time scale for normalization is $\delta_0/\Delta U$

Simulation	σ^*_{fun}	σ^*_{sub}	t^*_p	$E_{fun,t_p}/E_{fun,0}$
$Fr_c = 0.4$	0.1528	0.1187	12.0	3.874
$Fr_c = 1.2$	0.1597	0.1186	2.5	1.825
Linear stability theory	0.1430	0.1230	N/A	N/A

analysis. At later times, the fundamental mode of $Fr_c = 1.2$ simulation stops growing at an earlier time than the one of $Fr_c = 0.4$ simulation. Thus, the maximum amplitude of the fundamental mode in $Fr_c = 1.2$ simulation is far less the one in $Fr_c = 0.4$ simulation. Waves are observed to radiate from the shear layer for $Fr_c = 1.2$, but not for $Fr_c = 0.4$. The vortical structures for $Fr_c = 1.2$ are more elongated. Such features are known to arise in compressible mixing layer with a high convective Mach number [14, 50]. A promising future research direction would be to to investigate the interaction of wave-large scale turbulence interaction in shallow flows, in particular, (1) the physical mechanism responsible for the formation of wave radiation or shocks; and (2) the development of flow instability, both linear and nonlinear, under high convective Froude number. In fact, [38, 39] has attempted in such directions.

7 Conclusion

The paper discusses the use of reduced dimensionality models and hydrodynamic stability theories to illuminate the large scale 2DCS dynamics of shallow shear flows. The onset of 2DCS for both wakes and mixing layers is well explained by the linear stability theory. For shallow wakes, the spatio-temporal perturbation dynamics is instrumental in further classifying the instabilities as being of absolute or convective type. In addition, for shallow flows with $S \to S_c$, weakly nonlinear theory is employed, where the Ginzburg–Landau equation is derived from the reduced dimensionality model and used to investigate the initial growth of the instability. For shallow mixing layers with $S \ll S_c$, the nonlinear mean-field theory is found to reveal the interaction between the coherent structures and the basic flow field and explain the formation of such structures. Once developed, the coherent structures in shallow mixing layers are themselves unstable and their dynamics is governed by secondary linear stability theory, which leads to the merging of the structures.

The role of gravity waves on the stability of shallow shear flows is best represented by the convective Froude number. When Fr_c is large, gravity wave radiation has a stabilizing effect on the shear instability. This is analogous to the way compressibility wave radiation is known to stabilize shear compressible flows when the convective Mach number is large. The coherent structures are elongated and small shocks (hydraulic jumps) occur near the saddle point of coherent structures. Such little shocks are called "shocklets" in the gas dynamics literature.

Further research can be directed to understand the respective roles of inverse energy cascade and hydrodynamic stability theories in 2DCS development. It is also worthwhile to investigate the development of flow instability in high convective Froude numbers and the physical mechanism responsible for the formation of wave radiation or shocks.

Acknowledgements The financial support by the Hong Kong Research Grant Council, Project No. T21-602/15R, is gratefully acknowledged.

References

1. Akkermans RAD, Cieslik AR, Kamp LPJ, Trieling RR, Clercx HJH, van Heijst GJF (2008) The three-dimensional structure of an electromagnetically generated dipolar vortex in a shallow fluid layer. Phys Fluids 20(116):601
2. Akkermans RAD, Holten APC, Kamp LPJ, Clercx HJH, van Heijst GJF (2012) Arrays of vortices in shallow fluids: three-dimensional structure and dispersion. Eur J Mech B Fluid 34:131–145
3. Alavian V, Chu VH (1985) Turbulent exchange flow in a shallow compound channel. In: Proceedings of the 21st IAHR Congress. Melbourne, Australia vol 3, pp 446–451
4. Bayly BJ, Orszag SA, Herbert T (1988) Instability mechanisms in shear-flow transition. Ann Rev Fluid Mech 20:359–391
5. Belan M, Tordella D (2002) Asymptotic expansions for two dimensional symmetrical laminar wakes. ZAMM 82:221–234
6. Bers A (1983) Handbook of plasma physics. North Holland, Amsterdam
7. Carmer CF (2005) Shallow turbulent wake flows: momentum and mass transfer due to large-scale coherent vortical structures. Ph.D. thesis, Karlsruhe Institute of Technology
8. Chan FC (2005) Investigation of water wakes in shallow environment. Master's thesis, HKUST
9. Chan F, Ghidaoui M, Kolyshkin A (2006) Can the dynamics of shallow wakes be reproduced from a single time-averaged profile? Phys Fluids 18(048):105
10. Chen D, Jirka GH (1995) Experimental study of plane turbulent wake in a shallow water layer. Fluid Dyn Res 16(1):11–41
11. Chen D, Jirka GH (1997) Absolute and convective instabilities of plane turbulent wakes in a shallow water layer. J Fluid Mech 338:157–172
12. Chen D, Jirka GH (1998) Linear stability analysis of turbulent mixing layers and jets in shallow water layers. J Hydraul Res 36(5):815–830
13. Chu VH, Wu JH, Khayat RE (1983) Stability of turbulent shear flows in shallow channel. In: Proceedings of the 20th IAHR Congress, Moscow, Russia vol 3, pp 128–133
14. Chu VH (2014) Instabilities in non-rotating and rotating shallow shear flows. Environ Fluid Mech 14(5):1085–1103
15. Chu VH, Babarutsi S (1988) Confinement and bed-friction effects in shallow turbulent mixing layers. J Hydraul Eng ASCE 114(10):1257–1274
16. Chu VH, Wu JH, Khayat R (1991) Stability of transverse shear flows in shallow open channels. J Hydraul Eng ASCE 117(10):1370–1388
17. Dean RG, Dalrymple RA (1991) Water wave mechanics for engineers and scientists. World Scientific, Singapore
18. Deissler RJ (1989) External noise and the origin and dynamics of structure in convectively unstable systems. J Stat Phys 54(5/6):1459–1487
19. Dracos T, Giger M, Jirka GH (1992) Plane turbulent jets in a bounded fluid layer. J Fluid Mech 241:587–614
20. Drazin PG (2002) Introduction to hydrodynamic stability. Cambridge University Press, Cambridge
21. Falques A, Iranzo V (1994) Numerical simulation of vorticity waves in the nearshore. J Geophys Res 99(C1):825–841
22. Gaster M (1962) A note on the relation between temporally-increasing and spatially-increasing disturbances in hydrodynamic stability. J Fluid Mech 14:222–224
23. Ghidaoui MS, Kolyshkin AA (1999) Linear stability analysis of lateral motions in compound channels with free surface. J Hydraul Eng ASCE 125(8):871–880
24. Ghidaoui MS, Deng JQ, Gray WG, Xu K (2001) A boltzmann based model for open channel flows. Int J Com Fluid Dyn 20(6):436–451
25. Ghidaoui MS, Kolyshkin AA, Chan FC, Liang JH, Xu K (2006) Linear and nonlinear analysis of shallow wakes. J Fluid Mech 548:309–340
26. Ghidaoui M, Kolyshkin A (2004) On the spatial stability of shallow mixing layers. In: Proceedings of the 10th Asian congress on fluid mechanics, Pedadenyar, Sri Lanka (in CD)
27. Godreche C, Manneville P (1998) Hydrodynamics and nonlinear instabilities. Cambridge University Press, Cambridge

28. Grohne D (1969) Die stabilitat der ebenen kanalstromung gegenuber dreidimensionalen storungen von endlicher amplitude. Technical report 69-A-30, AVA Gottingen Rep
29. Grubišič V, Smith R, Schär C (1995) The effect of bottom friction on shallow-water flow past an isolated obstacle. J Atmos Sci 52:1985–2005
30. Hinterberger C, Frohlich J, Rodi W (2007) Three-dimensional and depth-averaged large-eddy simulations of some shallow water flows. J Hydraul Eng ASCE 133(8):857–872
31. Ho CM, Huang LS (1982) Subharmonics and vortex merging in mixing layers. J Fluid Mech 119:443–473
32. Ho CM, Huerre P (1984) Perturbed free shear layers. Ann Rev Fluid Mech 16:365–424
33. Huerre P, Monkewitz PA (1990) Local and global instabilities in spatially developing flows. Ann Rev Fluid Mech 22:473–537
34. Ingram RG, Chu VH (1987) Flow around islands in Rupert Bay: an investigation of the bottom friction effect. J Geophys Res 92:14521–14533
35. Jirka GH, Uijttewaal WSJ (2004) Shallow flows: a definition. In: Jirka G, Uijttewaal WSJ (eds) Shallow flows: selected papers of the international symposium on shallow flows, 16–18 June 2003. Taylor and Francis, pp 3–11
36. Jirka GH (2001) Large scale flow structures and mixing processes in shallow flows. J Hydraul Res 39(6):567–573
37. Jirka GH, Seol DG (2010) Dynamics of isolated vortices in shallow flows. J Hydro-environ Res 4:65–73
38. Karimpour S, Chu VH (2016) Instability of unbounded transverse mixing layer in shallow waters. Can J Civ Eng 43:504–510
39. Karimpour S, Chu VH (2019) The role of waves on mixing in shallow waters. Can J Civ Eng 46:134–147
40. Kelly RE (1967) On the stability of an inviscid shear layer which is periodic in space and time. J Fluid Mech 27:657–689
41. Kimura I, Uijttewaal WSJ, Hosoda T, Ali MS (2009) Urans computations of shallow grid turbulence. J Hydraul Eng ASCE 135(2):118–131
42. Klaassen GP, Peltier WR (1989) Role of transverse secondary instabilities in the evolution of free shear layers. J Fluid Mech 202:367–402
43. Koch W (1985) Local instability characteristics and frequency determination of self-excited wake flows. J Sound Vib 99:53–83
44. Kolyshkin AA, Ghidaoui MS (2002) Gravitational and shear instabilities in compound and composite channels. J Hydraul Eng ASCE 128(12):1076–1086
45. Kolyshkin AA, Ghidaoui MS (2003) Stability analysis of shallow wake flows. J Fluid Mech 494:355–377
46. Kraichnan R (1967) Inertial ranges in two-dimensional turbulence. Phys Fluids 10:1417–1428
47. Lam MY, Ghidaoui MS (2015) Secondary instability of two-dimensional coherent structures in shallow mixing layers. In: Proceedings of the 36th IAHR congress, The Hague, The Netherlands
48. Lam MY (2015) The development of shallow mixing layers: the roll-up and merging of large scale coherent structures. Ph.D. thesis, HKUST
49. Lam MY, Ghidaoui MS, Kolyshkin AA (2016) The roll-up and merging of coherent structures in shallow mixing layers. Phys Fluids 28(094):103
50. Lesieur M (2008) Turbulence in fluids, 4th edn. Springer, Dordrecht
51. Liang JH (2006) Linear and nonlinear analysis of shallow mixing layers. Master's thesis, HKUST
52. Lima A, Izumi N (2014) Linear stability analysis of open-channel shear flow generated by vegetation. J Hydraul Eng 140:231–240
53. Lloyd PM, Stansby PK (1997) Shallow-water flow around model conical islands of small side slope. I: Surface piercing. J Hydraul Eng ASCE 123(12):1057–1067
54. Maurel A, Pagneux V, Wesfreid JE (1995) Mean-flow correction as non-linear saturation mechanism. Europhys Lett 32(3):217–222
55. Meksyn D, Stuart JT (1951) Stability of viscous motion between parallel planes for finite disturbances. Proc R Soc Lond A 208:517–526
56. Metcalfe RW, Orszag SA, Brachet ME, Menon S, Riley JJ (1987) Secondary instability of a temporally growing mixing layer. J Fluid Mech 184:207–243
57. Negretti ME, Vignoli G, Tubino M, Brocchini M (2006) On shallow-water wake: an analytical study. J Fluid Mech 567:457–475
58. Patnaik PC, Sherman FS, Corcos GM (1976) A numerical simulation of Kelvin–Helmholtz waves of finite amplitude. J Fluid Mech 73:215–240

59. Pier B (2002) On the frequency selection of finite-amplitude vortex shedding in the cylinder wake. J Fluid Mech 458:407–417
60. Pier B, Huerre P (2001) Nonlinear self-sustained structures and fronts in spatially developing wake flows. J Fluid Mech 435:145–174
61. Pierrehumbert RT, Widnall SE (1982) Two- and three-dimensional instability of a spatially periodic shear layer. J Fluid Mech 114:59–82
62. Provansal M, Mathis C, Boyer L (1987) Benard-von Karman instability: transient and forced regimes. J Fluid Mech 182:1–22
63. Riley JJ, Metcalfe RW (1980) Direct numerical simulation of a perturbed turbulent mixing layer. In: AIAA 18th aerospace meeting, Pasadena, CA, AIAA reprint, pp 80–0274
64. Schmid PJ, Henningson DS (2001) Stability and transition in shear flows. Springer, New York
65. Singh L, Bandi M, Mahadevan A, Mandrei S (2016) Linear stability analysis for monami in a submerged seagrass bed. J Fluid Mech 786:642
66. Socolofsky SA, Jirka GH (2004) Large-scale flow structures and stability in shallow flows. J Environ Eng Sci 3(5):451–462
67. Stuart JT (1967) On finite amplitude oscillations in laminar mixing layers. J Fluid Mech 29:417–440
68. Tordella D, Belan M (2003) A new matched asymptotic expansion for the intermediate and far flow behind a finite body. Phys Fluids 15:1897–1906
69. Uijttewaal WSJ, Booij R (2000) Effect of shallowness on the development of free-surface mixing layers. Phys Fluids 12(2):392–402
70. Uijttewaal WSJ, Jirka GH (2003) Grid turbulence in shallow flows. J Fluid Mech 489:325–344
71. van Prooijen BC (2004) Shallow mixing layers. Ph.D. thesis, Delft University of Technology
72. van Prooijen BC, Uijttewaal WSJ (2002) A linear approach for the evolution of coherent structures in shallow mixing layers. Phys Fluids 14(12):4105–4114
73. van Prooijen BC, Uijttewaal WSJ (2009) The relevance of a back-scatter model for depth-averaged flow simulation. Flow Turbul Combust 82(1):73–91
74. Vreugdenhil CB (1994) Numerical methods for shallow-water flow. Kluwer Academic Press, Dordrecht
75. Wolanski EJ, Imberger J, Heron ML (1984) Island wakes in shallow coastal waters. J Geophys Res 89:10553–10569